Proceedings of the 2005 IEEE
International Conference on Robotics and Automation
Barcelona, Spain, April 2005

Potential Field Navigation of High Speed Unmanned Ground Vehicles on Uneven Terrain

Shingo Shimoda, Yoji Kuroda and Karl Iagnemma
Department of Mechanical Engineering, Massachusetts Institute of Technology
Cambridge, MA USA
sshimoda@mit.edu

***Abstract*-This paper proposes a potential field-based method for high speed navigation of unmanned ground vehicles (UGVs) on uneven terrain. A potential field is generated in the two-dimensional "trajectory space" of the UGV path curvature and longitudinal velocity. Dynamic constraints, terrain conditions, and navigation conditions can be expressed in this space. A maneuver is chosen within a set of performance bounds, based on the potential field gradient. In contrast to traditional potential field methods, the proposed method is subject to local maximum problems, rather than local minimum. It is shown that a simple randomization technique can be employed to address this problem. Simulation and experimental results show that the proposed method can successfully navigate a UGV between pre-defined waypoints at high speed, while avoiding unknown hazards. Further, vehicle velocity and curvature are controlled to avoid rollover and excessive side slip. The method is computationally efficient, and thus suitable for on-board real-time implementation.**

Index Terms – UGVs, Autonomous control, Potential field.

I. Introduction

Unmanned ground vehicles are expected to play significant roles in future military, planetary exploration, and materials handling applications [1,2]. Many applications require UGVs to move at high speeds on unknown, rough terrain. During high speed navigation, dynamic hazards such as vehicle rollover and side slip must be avoided. In addition, UGVs moving at high speed will likely encounter unexpected hazards at short range. To avoid these hazards, navigation algorithms must be computationally efficient while still considering important vehicle dynamics and problem constraints.

Artificial potential fields have long been successfully employed for robot control and motion planning. First works were performed by Khatib as a real-time obstacle avoidance method for manipulators [3]. Ge et al. applied a potential field method for dynamic control of a mobile robot, with moving obstacles and goal [4]. Latombe applied potential field methods to general robot path planning [5]. Path planning using artificial potential field has also been applied to parallel computation schemes and nonholonomic systems [6,7]. Potential field navigation for wheeled robots on natural terrain has also been explored [8]. In general, potential field methods have been used for planning and control of low-speed systems on flat terrain. Here we propose a method for navigation of high speed vehicles on uneven terrain.

In conventional methods, potential fields are often defined in Cartesian space. This is attractive because it is intuitively easy to define potential "source" and "sink" functions for obstacles and goals in such a space. A vehicle then navigates from points of high potential to those of low potential. One problem of such an approach is that often only the navigation conditions (such as goal and obstacle locations) are used to define the potential field.

In the proposed method, the potential field is defined in the two-dimensional "trajectory space" of the robot path curvature and longitudinal velocity [9]. Dynamic constraints due to rollover and side slip, terrain conditions, and navigation conditions (such as waypoint location(s), goal location, hazard location(s) and desired velocity) can easily be expressed as potential functions in the trajectory space. A maneuver is chosen within a set of performance bounds, based on the potential field gradient. This yields a desired value for the UGV path curvature and velocity. Desired values for steering angle and throttle can then be computed and used as inputs to low-level controllers.

II. Trajectory Space Description and Assumptions

A. Trajectory Space Description

The trajectory space is defined as a two-dimensional space of a UGV's instantaneous path curvature and longitudinal velocity, as shown in Fig. 1(a) [9]. A point in the trajectory space serves as a physically intuitive description of the current vehicle status. This space clearly does not describe the complete vehicle state, but rather captures simple but important UGV kinematic values. The relationship of a point in the trajectory space and a vehicle maneuver is shown in Figs. 1 (a) and (b).

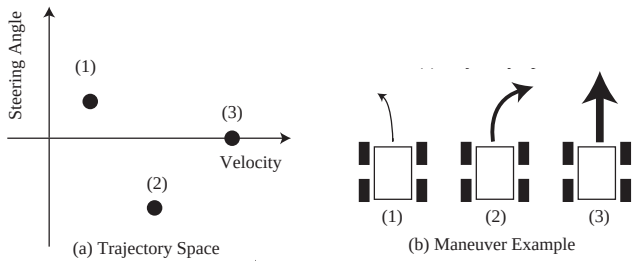

Fig. 1. Trajectory space description and maneuver example.

The trajectory space is a convenient space for navigation for two reasons. First, the trajectory space maps easily to the UGV actuation space (generally consisting of the throttle and steering angle). Navigation algorithms performed in the trajectory space will select command inputs

that obey vehicle nonholonomic constraints. Second, dynamic constraints related to UGV rollover and side slip are easily expressible in the trajectory space, since these constraints are functions of the UGV velocity and path curvature. These constraints can also capture effects such as terrain inclination and roughness. To perform navigation, a potential field is first constructed in the trajectory space. This is discussed below.

B. Problem Assumptions

During high speed navigation, a UGV must rapidly select steering and throttle inputs to navigate between waypoints toward a goal location, while avoiding discrete hazards, rollover, or excessive side slip. In the assumed scenario such waypoints might be designated *a priori* from relatively coarse elevation data (such as from a topographical map). Hazards would be detected from on-board range sensors, and might take the form of terrain discontinuities such as rocks or ditches, or non-geometric hazards such as soft soil. Hazard detection and sensing issues are not a focus of this work. Here we assume knowledge of waypoint, goal, and hazard locations. We also assume that local terrain inclination and roughness can be sensed or estimated.

The coordinate systems are shown in Fig. 2. A body frame ***B*** is fixed to the vehicle, with its origin at the vehicle center of mass. The position of the vehicle in the inertial frame ***I*** is expressed as the position of the origin of ***B***. The vehicle attitude is expressed by *x*-*y*-*z* Euler angles using the vehicle yaw θ, roll ϕ, and pitch ψ defined in ***B***.

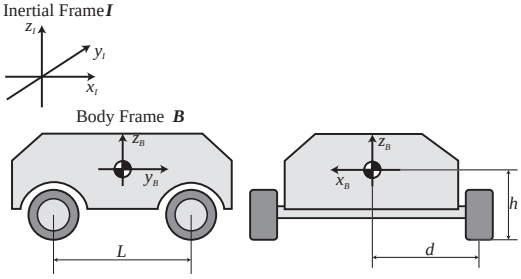

Fig. 2. Definition of coordinate system.

III. Potential Field Definition

In the proposed method, individual potential fields are constructed for each constraint and goal. The sum of all potential fields is then used for control. Here we define potential functions for the rollover and side slip constraints, waypoints (and goal) locations, hazard locations, and the desired UGV velocity.

A. Potential Field for Rollover and Side Slip Constraints

UGV rollover and side slip constraints are computed from low-order dynamic models. A simple rollover constraint for a UGV on uneven terrain can be expressed as:

$$\rho_r(v) = \sin^{-1}\left(L\frac{dg_z \pm hg_x}{gv^2} \right) \tag{1}$$

where

ρ_r: Maximum allowable steering angle
v: Vehicle velocity
g_*: Gravitational acceleration of *-axis direction in ***B***
L: UGV length
d: UGV half-width (see Fig. 2)
h: Height of UGV c.g. from ground (see Fig. 2)

The two solutions to (1) correspond to downhill/uphill travel. A potential field is then defined as:

$$PF_r(v,\rho) = \begin{cases} K_r\left(1 - \dfrac{(\rho-\rho_{MAX})^2}{(\rho_r(v)-\rho_{MAX})^2}\right) & \rho_r < |\rho| < \rho_{MAX} \\ 0 & 0 < |\rho| < \rho_r \end{cases} \tag{2}$$

where

ρ: Steering angle
ρ_{MAX}: Steering angle mechanical limit

Here, K_r is a positive gain parameter to modulate the potential field height. An illustration of a potential field for the UGV rollover constraint is shown in Fig. 3.

A simple side slip constraint for a UGV on uneven terrain can be expressed as follows:

$$\rho_s(v) = \sin^{-1}\left(L\frac{-g_x \pm \mu g_z}{v^2} \right) \tag{3}$$

where

ρ_s: Maximum allowable steering angle
μ: Terrain tractive coefficient

A potential field is then defined as:

$$PF_s(v,\rho) = \begin{cases} K_s\left(1 - \dfrac{(\rho-\rho_{MAX})^2}{(\rho_s(v)-\rho_{MAX})^2}\right) & \rho_s < |\rho| < \rho_{MAX} \\ 0 & 0 < |\rho| < \rho_s \end{cases} \tag{4}$$

Again, K_s is a positive gain parameter to modulate the potential field height. An illustration of a potential field for the side slip constraint appears similar to that for the rollover constraint shown in Fig. 3. Note that rollover and side slip constraints are affected by terrain roughness. Detailed discussion of this effect is omitted here for brevity.

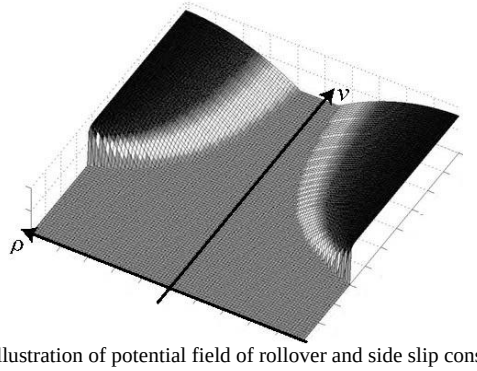

Fig. 3. Illustration of potential field of rollover and side slip constraints.

B. Potential Field for Waypoint Locations

For UGV navigation between waypoints, a desired velocity and steering angle must be computed at each instant based (at minimum) on the relative location of the UGV and the waypoint. Consider a UGV moving toward a desired waypoint as shown in Fig. 4. Possible paths to the waypoint are shown as Paths A and B. Both paths have the same initial steering angle. However Path B is more direct

and thus more desirable (in the absence of other constraints) than Path A.

To generate similar desirable steering angles, we propose a method illustrated in Fig. 5. Here a line connecting the UGV and the waypoint intersects with a circle centered at the UGV c.g. The radius of the circle is equal to the diameter of a circle with curvature ρ_{MAX}. The desired steering angle is taken as the angle to the intersection point.

A potential field corresponding to the current desired waypoint location is then defined as follows:

$$PF_g(\rho) = K_g(\rho - \rho_d)^2 \quad (5)$$

where

ρ_d: Desired steering angle

K_g is a positive gain parameter to modulate the potential field height. An illustration of a potential field for waypoint location is shown in Fig. 6.

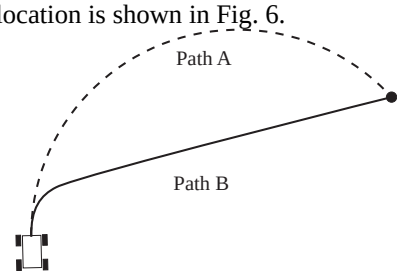

Fig. 4. Comparison of possible UGV paths toward a waypoint.

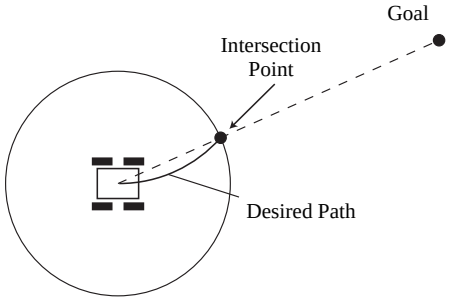

Fig. 5. Definition of desired steering angle.

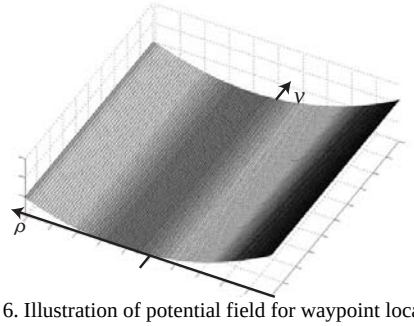

Fig. 6. Illustration of potential field for waypoint location.

C. Potential Field for Desired Velocity

The potential field for the desired UGV velocity is simply expressed as follows:

$$PF_v(v) = K_{v1}(v - v_d)^{Kv2} \quad (6)$$

where

v_d: Desired velocity

K_{v1} and K_{v2} are positive gain parameters to modulate the potential field height. v_d may be a function of position to reflect mission-level objectives. An illustration of the potential field for the desired velocity is shown in Fig. 7.

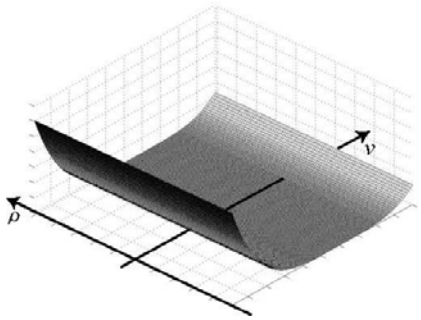

Fig. 7. Illustration of potential field of desired velocity.

D. Potential Field for Hazard Locations

Consider a UGV and a discrete hazard as shown in Fig. 8. Here ρ_1 and ρ_2 are the maximum and minimum steering angles toward the hazard. The potential field for hazard location is constructed considering the following:

- Steering angles between ρ_1 and ρ_2 are undesirable yet can be safely employed until the UGV is near the hazard;
- The potential field value should be higher at high speed than at low speed since control accuracy generally decreases with increasing speed;
- The locations of waypoints should influence the hazard potential field value, as illustrated in Fig. 9.

From these observations, a potential field for hazard locations is defined as follows:

$$PF_o(v,\rho) = \frac{K_o(K_{ov}v+1)}{(K_{od}O_d+1)(K_{oa}A_d+1)}\exp\left(-\frac{(\rho - X)^2}{2\sigma}\right) \quad (7)$$

where

O_d: Euclidean distance between vehicle and hazard

A_d: Angle between heading and waypoint location

X: $(\rho_1 + \rho_2)/2$

σ: $(\rho_1 - \rho_2)/2$

K_o, K_{od}, K_{oa}, and K_{ov} are positive gain parameters to modulate the potential field height. An illustration of the potential field for hazard location is shown in Fig. 10.

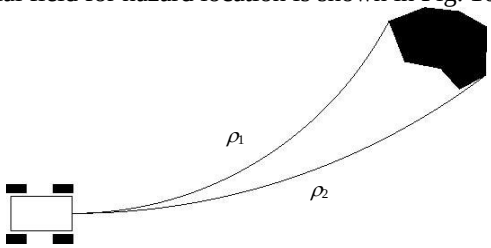

Fig. 8. Minimum and maximum steering angle towards a hazard.

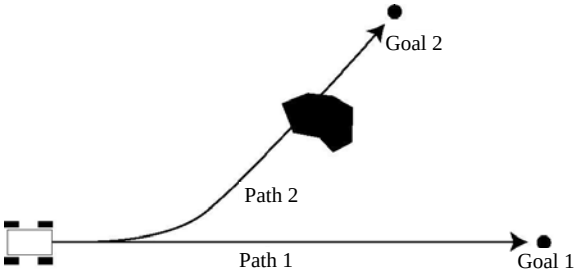

Fig. 9. Influence of relative locations of waypoints and hazards.

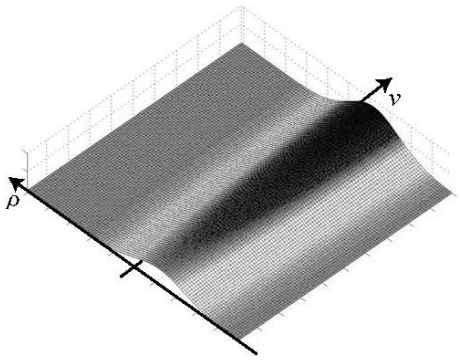

Fig. 10. Illustration of potential field of hazard location.

E. Definition of Net Potential Field

A net potential field is generated as the sum of all the proposed potential fields, as follows:

$$PF(v,\rho) = PF_r(v,\rho) + PF_s(v,\rho) + PF_g(\rho) + PF_v(v) + PF_o(v,\rho) \quad (8)$$

An illustration of the net potential field is shown in Fig. 11.

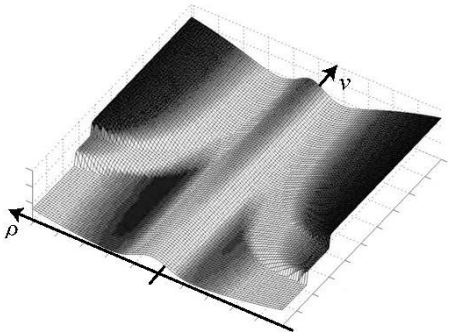

Fig. 11. Illustration of proposed net potential field.

F. Potential Field Trajectory Space Navigation

In conventional potential field methods, the direction of desired motion at a given instant is determined by computing the gradient of the potential field at the current point and moving in the direction of maximum descent. In the proposed method not only the gradient at the current point but also the gradient at the next point, that is, the desired velocity and the curvature are important. Further, the potential field gradient is computed over a space determined from UGV performance bounds. This is due to the constraint that the chosen maneuver (i.e. path curvature and velocity) must be attainable within one control cycle. Fig. 12(a) shows an example of a region in the trajectory space that is attainable in one control cycle for a UGV. This region is defined by UGV performance bounds on acceleration/deceleration and steering rate. Details related to computation of these bounds are omitted here for brevity. The region is here discretized into nine equally-spaced squares, though other discretization geometries and resolutions are possible.

1. A maneuver is chosen as follows:
2. 1. The value of the net potential field at the center of each discrete square is calculated as illustrated in Fig. 12(b);
3. 2. To save calculation time for real time response, a plane fit to the elevations is performed and the gradient is calculated. The direction of maximum descent is taken as the desired maneuver direction;
4. 3. The desired velocity and steering angle are computed as the values on the attainable region boundary in the direction of the desired maneuver from the current point.

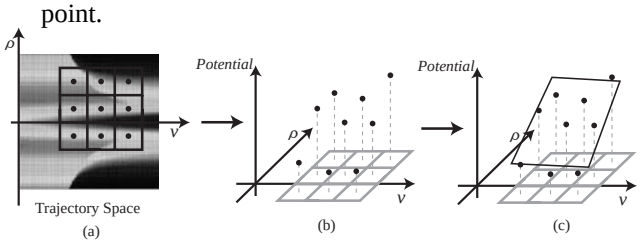

Fig. 12. Influence of performance bounds on maneuver selection.

IV. Local Minimum Problem Discussion

A. Conventional Local Minimum Description

The existence of local minima is a fundamental problem associated with potential fields constructed from numerous potential functions. A classical local minimum problem is shown in Fig. 13. For the given locations of hazard and waypoint, Area A is a possible location of a local minimum, and thus a region where an algorithm might (wrongly) direct a UGV.

A second situation is shown in Fig. 14. Here the waypoint (goal) is located between the UGV and an hazard, and the waypoint lies within the region of influence of the hazard. In this case the global minimum of the potential field is not the waypoint position. A UGV might reach this global minimum yet not reach the waypoint. This situation is called a "free-path local minimum."

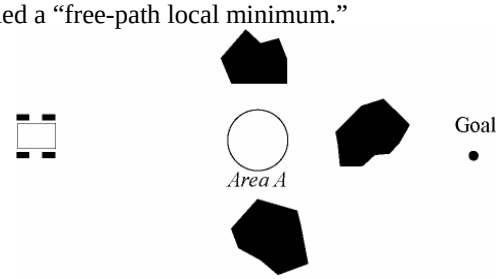

Fig. 13. Example of conventional local minimum.

Fig. 14. Example of conventional free-path local minimum.

B. Trajectory Space Local Maximum Description

Situations that lead to local minimum situations in classical potential field approaches often lead to local maximum situations in the proposed method. For example, Fig. 15 shows a situation similar to that shown in Fig. 13, with a corresponding trajectory space potential field. It can be seen that due to the symmetry of the potential field and the definition of the hazard and waypoint potential functions, the field gradient is zero and the desired maneuver would (incorrectly) direct the UGV toward the hazard.

In practice, local maxima are unlikely to occur due to sensor noise, terrain unevenness, etc. However to address the issue Gaussian random noise of small amplitude is added to each discrete element in the attainable region of

the trajectory space described in Section III(E). This serves to perturb unstable local maxima, and avoid situations such as that shown in Fig. 15. In "normal" operation, the addition of random noise does not significantly affect navigation performance.

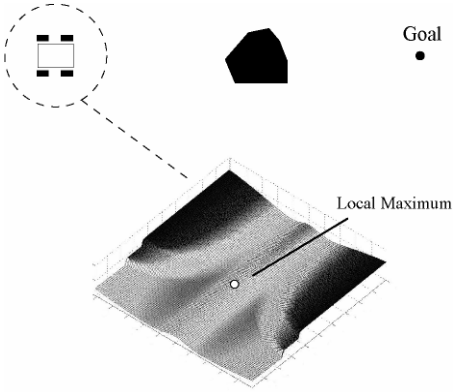

Fig. 15. Example of trajectory space local maximum.

An example of the effect of this method is shown in Fig. 16. Here a situation similar to that shown in Fig. 13 is presented. Here, however, the addition of noise causes the UGV to avoid the hazards and navigate toward the goal.

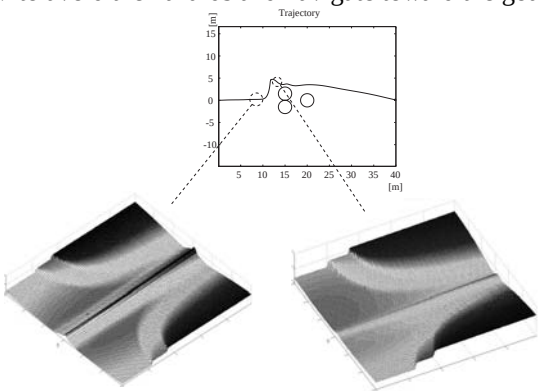

Fig. 16. Example of local maximum avoidance by addition of noise.

V. Simulation Results

Extensive simulations were conducted of a small UGV traveling at high speeds over uneven terrain using the multibody dynamic simulation software ADAMS. UGV parameters were set as:

UGV length L = 0.27 m
UGV half-width d = 0.124 m
Height of UGV c.g. from ground h = 0.055 m
Wheel diameter = 0.12 m
K_r = 800, K_s = 800, K_g = 0.3, K_{v1} = 0.5 x 10^{-5}, K_{v2} = 4
K_o = 1500, K_{od} = 0.05, K_{oa} = 10, K_{ov} = 0.07

Rough terrain with fractal number of 2.05, grid spacing of 2 wheel diameters, and height scaling of 35 wheel diameters was employed. A map of a representative simulation is shown in Fig. 17. Hazard locations were (x,y) = (15.0, 0.0) and (x,y) = (50.0, 22.0) and waypoints were set at (x,y) = {(30.0, 0.0), (40.0, 20.0), (60.0, 20.0)}. PD control was employed for steering angle and velocity control.

A representative simulation result is shown in Figs. 18-19. Fig. 18 shows the UGV trajectory and shape of the potential field at several points. The vehicle navigated between all waypoints while avoiding both hazards. Fig. 19 shows that the velocity was controlled near the desired value of 5.0 m/s except during turns of large curvature. During these events the rollover and/or side slip potential functions caused the velocity to decrease. Fig. 19 shows plots of the UGV roll angle and slip angle during the trajectory, illustrating the effectiveness of the algorithm in minimizing these quantities.

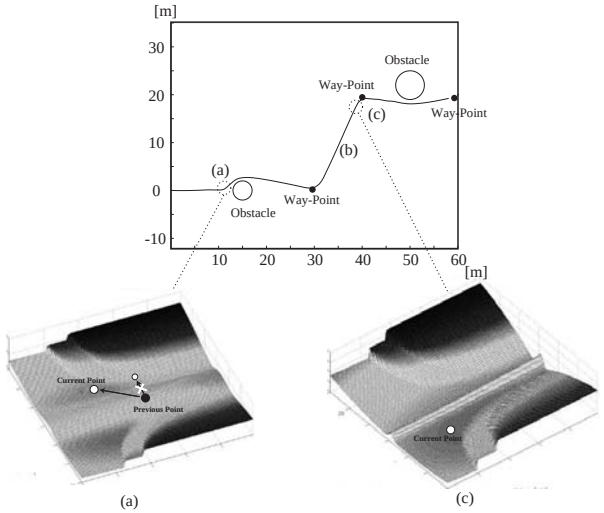

Fig. 17. Map and sample trajectory spaces of simulation result.

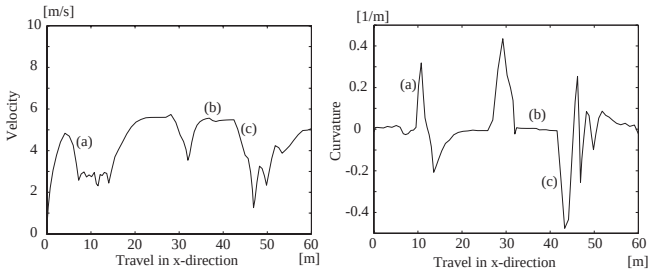

Fig. 18. UGV velocity and curvature—simulation results.

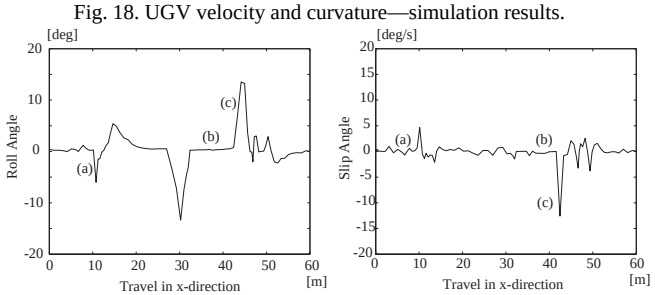

Fig. 19. UGV Roll angle and slip angle—simulation results.

VI. Experimental Results

The experimental UGV ARTEMIS is shown in Fig. 20. ARTEMIS is equipped with a Zenoah G2D70 gasoline engine, 700 MHz Pentium III PC -104 onboard computer, Crossbow AHRS-400 INS, a tachometer to measure wheel angular velocity, 20 cm resolution DGPS, and Futaba steering and throttle control servos. The UGV dimensions are 0.89 x 0.61 x 0.38 m. Experiments were conducted on flat, bumpy terrain covered with grass. In each experiment, the UGV initial position was the origin of the inertial frame, with initial heading aligned with the x axis.

First experiments were conducted to study high speed hazard avoidance. A hazard of 1 m radius was set at (x,y) =

(15.0, 0.0) and a waypoint was set at (x,y) = (30.0, 0.0). The desired velocity was set at 4.0 m/s. Note that for a vehicle of this size, rollover can easily occur at 4.0 m/s.

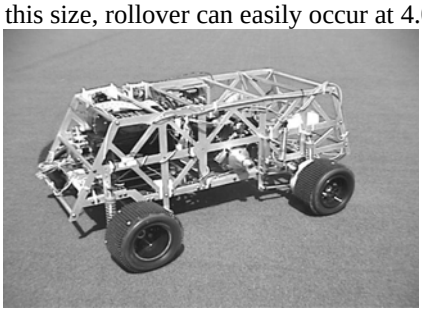

Fig. 20. ARTEMIS Experimental UGV.

An experimental result is shown in Figs. 21 and 22. The UGV trajectory is shown in Fig. 21. The UGV successfully avoided the hazard and reached the waypoint. Initial heading error was caused by GPS offset. UGV velocity and curvature are shown in Fig. 22. The velocity was controlled to decrease at periods of large curvature (i.e. around x = 15.0 m) and controlled to near 4.0 m/s in "safe" regions (i.e. after x = 25.0 m). Finally, the vehicle navigated without rollover or side slip. Each computation cycle, involving construction of the net potential field and selection of a maneuver, required approximately 50 ms.

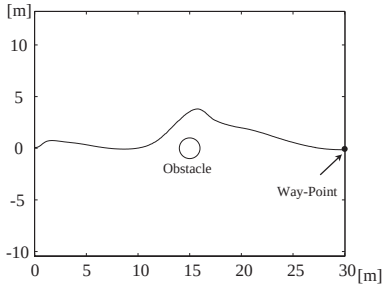

Fig. 21. GPS Trajectory of hazard avoidance experiment.

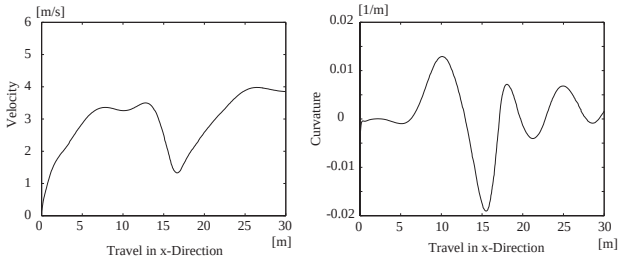

Fig. 22. Velocity and curvature of hazard avoidance experiment.

Other experiments were conducted to study high speed navigation between multiple waypoints. Three waypoints were set at (x,y) = {(25.0, 0.0), (30.0, 10.0), (40.0, 10.0)}. The desired velocity was 4.0 m/s. The target waypoint was indexed when the UGV moved to within 2.0 m of the current waypoint.

An experimental result is shown in Figs. 23 and 24. Fig. 23 shows that the vehicle successfully navigated between waypoints. Fig. 24 shows that the velocity was controlled near 4.0 m/s, and decreased during periods of large curvature.

These results suggest that the proposed method can be used for real time navigation of a UGV at high speeds. Current research involves experimental validation of the method on steeply sloped and highly rough outdoor terrain.

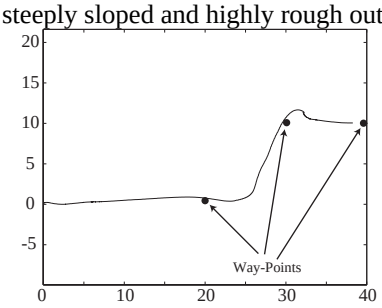

Fig. 23. Trajectory of waypoints navigation experiment.

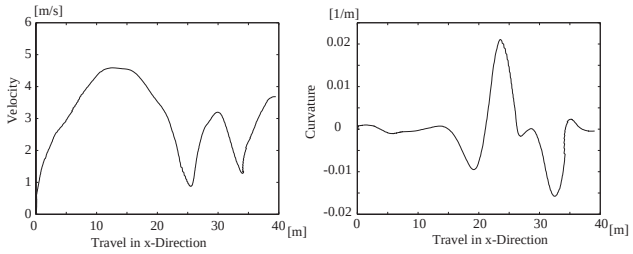

Fig. 24. Velocity and curvature of waypoint navigation experiment.

VI. Conclusion

This paper has presented a novel potential field-based method for high speed navigation of UGVs on rough terrain. Dynamic constraints, terrain conditions, and navigation conditions can be expressed in this space. A maneuver is chosen within a set of performance bounds, based on the potential field gradient. Issues related to local minima and maxima were discussed, and it was shown that a simple randomization technique can be employed to address this problem. Simulation and experimental results demonstrated the effectiveness of the method. The method is extremely computationally efficient, and thus suitable for onboard real-time implementation. Navigation over rough and slippery terrain is a topic of current study.

References

[1] J. Walker, "Unmanned Ground Combat Vehicle Contractors Selected," *DARPA News Release*, February 7, 2001, (www.darpa.mil)

[2] G. Gerhart, R. Goetz, D. Gorsich, "Intelligent Mobility for Robotic Vehicles in the Army after Next," *Proceedings of the SPIE Conference on Unmanned Ground Vehicle Technology*, 1999

[3] O. Khatib, "Real-time Obstacle Avoidance for Manipulators and Mobile Robots," *International Journal of Robotics Research*, Vol. 5, No. 1, pp. 90-98, 1986

[4] S. Ge and Y. Cui, "Dynamic Motion Planning for Mobile Robots Using Potential Field Method," *Autonomous Robots*, Vol. 13, 2002

[5] J. Barraquand and B. Langlois and J. Latombe, "Numerical Potential Field Techniques for Robot Path Planning," *IEEE Trans. on Systems, Man, and Cybernetics*, Vol. 22, No.2, pp. 224-241, 1992

[6] S. Caselli, M. Reggiani, and R. Sbravati, "Parallel Path Planning with Multiple Evasion Strategies," *Proceedings of the IEEE International Conference on Robotics and Automation*, pp. 1232-1237, 2002

[7] H. Tanner, S. Loizou, and K. Kyriakopoulos, "Nonholonomic Navigation and Control of Cooperating Mobile Manipulators," *IEEE Transaction on Robotics and Automation*, Vol. 19, No. 1, 2003

[8] H. Haddad, M. Khatib, S. Lacroix and R. Chatila., "Reactive Navigation in Outdoor Environments using Potential Fields," *Proceedings of the Intl. Conf. on Robotics and Automation*, pp. 1232-1237, 1998

[9] M. Spenko, K. Iagnemma, and S. Dubowsky, "High Speed Hazard Avoidance for Mobile Robots in Rough Terrain," *Proceedings of the SPIE Conference on Unmanned Ground Vehicles*, 2004